Check for updates

JGR Biogeosciences

RESEARCH ARTICLE
10.1029/2023JG007876

Nitrification in a Subterranean Estuary: An Ex Situ and In Situ Method Comparison Determines Nitrate Is Available for Discharge

Stephanie J. Wilson[1,2], Bongkeun Song[2], Iris C. Anderson[2], and Craig R. Tobias[3]

[1]Smithsonian Environmental Research Center, Edgewater, MD, USA, [2]Virginia Institute of Marine Science, College of William & Mary, Gloucester Point, VA, USA, [3]Department of Marine Sciences, University of Connecticut, Avery Point, Groton, CT, USA

Key Points:

- Nitrification in the subterranean estuary was observed with both ex situ and in situ measurement methods
- Ex situ incubation experiments revealed higher nitrification rates than in situ tracer or mixing model calculations
- Nitrate produced in the subterranean estuary may be exported to overlying coastal waters via submarine groundwater discharge

Supporting Information:

Supporting Information may be found in the online version of this article.

Correspondence to:

S. J. Wilson,
wilsonsj@si.edu

Citation:

Wilson, S. J., Song, B., Anderson, I. C., & Tobias, C. R. (2024). Nitrification in a subterranean estuary: An ex situ and in situ method comparison determines nitrate is available for discharge. *Journal of Geophysical Research: Biogeosciences*, *129*, e2023JG007876. https://doi.org/10.1029/2023JG007876

Received 27 OCT 2023
Accepted 16 MAY 2024

Author Contributions:

Conceptualization: Stephanie J. Wilson, Bongkeun Song, Iris C. Anderson, Craig R. Tobias
Data curation: Stephanie J. Wilson
Formal analysis: Stephanie J. Wilson
Funding acquisition: Bongkeun Song, Iris C. Anderson, Craig R. Tobias
Investigation: Stephanie J. Wilson, Craig R. Tobias
Methodology: Stephanie J. Wilson, Bongkeun Song, Craig R. Tobias
Project administration: Bongkeun Song, Iris C. Anderson, Craig R. Tobias
Resources: Craig R. Tobias
Supervision: Bongkeun Song, Iris C. Anderson, Craig R. Tobias
Visualization: Stephanie J. Wilson

© 2024. The Author(s).
This is an open access article under the terms of the Creative Commons Attribution License, which permits use, distribution and reproduction in any medium, provided the original work is properly cited.

Abstract Subterranean estuaries (STEs) form in the subsurface where fresh groundwater and seawater meet and mix. Subterranean estuaries support a variety of biogeochemical processes including those transforming nitrogen (N). Groundwater is often enriched with dissolved inorganic nitrogen (DIN), and transformations in the STE determine the fate of that DIN, which may be discharged to coastal waters. Nitrification oxidizes ammonium (NH_4^+) to nitrate, making DIN available for N removal via denitrification. We measured nitrification at an STE, in Virginia, USA using in situ and ex situ methods including conservative mixing models informed by in situ geochemical profiles, an in situ experiment with $^{15}NH_4^+$ tracer injection, and ex situ sediment slurry incubations with $^{15}NH_4^+$ tracer addition. All methods indicated nitrification in the STE, but the ex situ sediment slurries revealed higher rates than both the in situ tracr experiment and mixing model estimations. Nitrification rates ranged 55.0–183.16 μmol N m^{-2} d^{-1} based on mixing models, 94.2–225 μmol N m^{-2} d^{-1} in the in situ tracer experiment, and 36.6–109 μmol N m^{-2} d^{-1} slurry incubations. The in situ tracer experiment revealed higher rates and spatial variation not captured by the other methods. The geochemical complexity of the STE makes it difficult to replicate in situ conditions with incubations and calculations based on chemical profiles integrate over longer timescales, therefore, in situ approaches may best quantify transformation rates. Our data suggest that STE nitrification produces NO_3^-, altering the DIN pool discharged to overlying water via submarine groundwater discharge.

Plain Language Summary Groundwater mixes with coastal waters in subterranean estuaries that form in the subsurface along coastlines. Groundwater supplies compounds to these systems including nutrients such as nitrogen. Within the subterranean estuary, nitrogen may be transformed, influencing its availability to microbes for removal, its flow through sediments to coastal waters, and its availability to primary producers. Here we measured nitrification, a critical nitrogen cycle process that transforms ammonium to nitrite/nitrate in a subterranean estuary. We used several methods to measure nitrification including mixing models that rely on measured nitrogen concentrations across the groundwater salinity gradient, an isotope labeled nitrogen experiment that allows for tracing of nitrogen in the subsurface over time, and laboratory incubations. All methods indicated active nitrification in the STE, but the laboratory incubations revealed higher rates than both the tracer injections and mixing model estimations. Our data suggest that tracer approaches field conditions and heterogeneity, but that incubations and mixing model estimates are useful for determining control points and net impacts of the subterranean estuary on groundwater, respectively. Nitrification alters the form of nitrogen that is transported to overlying water via submarine groundwater discharge and, therefore, may influence the impact of groundwater derived nitrogen on coastal biogeochemistry.

1. Introduction

As groundwater is transported to the coastal ocean, it passes through the subterranean estuary (STE), a transition zone along the land-ocean continuum where groundwater and seawater meet and mix (Moore, 1999). Groundwater, recirculated seawater, or a mixture of both in the STE can be released to the coastal ocean as submarine groundwater discharge (SGD) (Moore, 1999; Santos et al., 2021). Groundwater often serves a source of nitrogen (N) to coastal waters (Cho et al., 2018; Santos et al., 2021), where *N* is a limiting nutrient regulating ecosystem productivity (Nixon, 1995). *N* accumulates in groundwater along the subsurface flow-path, supplied by organic matter remineralization, atmospheric deposition, wastewater or septic leaks, and fertilizer leachate (Cole

Writing – original draft: Stephanie J. Wilson
Writing – review & editing: Bongkeun Song, Iris C. Anderson, Craig R. Tobias

et al., 1993, 2006; Valiela et al., 1997). Transport of *N* via SGD has been estimated to be on the same order of magnitude as riverine *N* inputs to the ocean (Cho et al., 2018; Wilson, Anderson, & Song, 2023), groundwater, therefore, represents an important pathway for nutrients to be transported across the land-sea interface.

STEs are recognized as important reaction zones where biogeochemical processes influence the concentration and speciation of redox-sensitive elements, nutrients, trace metals, and carbon (Anschutz et al., 2016; Beck et al., 2017; Robinson et al., 2018; Santoro, 2010; Santos et al., 2008). Subsurface conditions in STEs are highly variable, the result of shifting hydraulic gradients, tidal pumping, wave setup, and steep geochemical profiles (Abarca et al., 2013; Heiss et al., 2014; Robinson et al., 2014; Slomp & Cappellen, 2004). This variability drives biogeochemical cycling within STEs, which is especially important to groundwater-derived N, as it determines the amount and form of N in SGD (Erler et al., 2014; Kroeger & Charette, 2008; Robinson et al., 2018; Santos et al., 2021; Wilson, Anderson, & Song, 2023). *N* transformations in these systems remain largely unconstrained and are often overlooked when estimating SGD fluxes (Beck et al., 2016; Cho et al., 2018). The biogeochemical reactions in the STE are central to determining the fate of groundwater-derived N and whether or not it is discharged to overlying waters (Moore et al., 2009) where SGD nutrients can promote primary production and compound coastal eutrophication (Santos et al., 2021; Valiela et al., 1990).

Within the STE, oscillating redox conditions can support a variety of *N* cycling reactions (Courtier et al., 2017 and citations therein; Santos et al., 2009). Remineralization of groundwater derived and surface water supplied organic matter can lead to ammonium (NH_4^+) production and, in some cases, accumulation (Kroeger & Charette, 2008). When groundwater enriched with ammonium (NH_4^+) encounters oxic zones, ammonia oxidizers can convert NH_4^+ to nitrite (NO_2^-), it may then be further oxidized to NO_3^-; collectively referred to here as nitrification. This process is of particular importance, considered a gate-keeping step in the *N* cycle, nitrification provides oxidized *N* to microbial *N* removal processes such as denitrification or anaerobic ammonium oxidation (anammox), which can significantly reduce groundwater *N* concentrations prior to discharge (Ward, 2013). Nitrification also influences the mobility of groundwater *N*, as NO_3^- is more mobile than NH_4^+ and may be more likely to be discharged (Böhlke et al., 2006). This process, therefore, influences the form and concentrations of N in STEs and that is exported to the coastal ocean via SGD.

Rates of nitrification can be estimated with both ex situ and in situ approaches. Isotope based approaches, such as isotope dilution or tracer methods, have become the standard for ex situ incubations allowing for the calculation of ambient or actual rates of nitrification (Jäntti et al., 2012; Lisa et al., 2015; Ward, 2011). Isotope tracer methods add ^{15}N-labeled NH_4^+, and follow its oxidation to $^{15}NO_2^-$ and $^{15}NO_3^-$ (collectively $^{15}NO_x$) as a measure of nitrification rates (Enoksson, 1986; Jäntti et al., 2012). This method is highly sensitive, but if not aerated properly $^{15}NO_x$ produced may be denitrified prior to measurement, and is considered a potential rate (Enoksson, 1986). To measure nitrification rates in the subsurface, the $^{15}NH_4^+$ approach has also been applied in situ in aquifers (Böhlke et al., 2006; Smith et al., 2006). The labeled plume is sampled over time and indicates the transport and fate of the conservative tracer and the ^{15}N-substrate, which can be measured in nitrification product pools (e.g., NO_x, N_2O, and N_2 when coupled to denitrification). Another approach, resulting in an in situ approximation of net nitrification, are conservative mixing curve calculations (Boyle et al., 1974; Officer & Lynch, 1981; Santos et al., 2009; Ullman et al., 2003). In the case of nitrification, salinity serves as a conservative tracer to assess non-conservative behavior of NH_4^+ and $^{15}NO_3^-$. These calculations estimate net rates integrated over water residence times and STE profiles.

Estimating process rates in STEs is difficult due to high variability in the subsurface and the complexity involved with replicating in situ conditions. Despite these difficulties, process rates are important to nutrient biogeochemistry in the coastal zone. Nitrification, and its potential coupling to denitrification or other *N* reduction pathways, is critical to understanding STE *N* cycling and *N* loading to coastal waters via SGD (Santos et al., 2021). Nutrient loading from groundwater has been identified as a contributor to coastal eutrophication and STE processes are a critical control on SGD fluxes (Santos et al., 2021; Wilson et al., 2024). The lack of rate estimations in STEs make it difficult to produce accurate nutrient flux estimates or develop constraints on STE transformations that could better our understanding of these complex systems and the role of nutrient loading via SGD in coastal biogeochemistry. In this study, we examined the fate of groundwater derived *N* in the sandy sediment Gloucester Point Beach STE, Virginia, USA. We employed both in situ and ex situ approaches including conservative mixing calculations, an in situ tracer experiment, and ex situ tracer incubations to estimate STE nitrification rates, compare methodological approaches for estimating STE transformations, and consider the

21698961, 2024, 6, Downloaded from https://agupubs.onlinelibrary.wiley.com/doi/10.1029/2023JG007876 by Viva Jmu Procurement Services, Wiley Online Library on [30/03/2025]. See the Terms and Conditions (https://onlinelibrary.wiley.com/terms-and-conditions) on Wiley Online Library for rules of use; OA articles are governed by the applicable Creative Commons License

21698961, 2024, 6, Downloaded from https://agupubs.onlinelibrary.wiley.com/doi/10.1029/2023JG007876 by Viva Jmu Procurement Services, Wiley Online Library on [30/03/2025]. See the Terms and Conditions (https://onlinelibrary.wiley.com/terms-and-conditions) on Wiley Online Library for rules of use; OA articles are governed by the applicable Creative Commons License

utility of these measurements in the context of SGD flux estimations. We hypothesized that ex situ incubations would over estimate while mixing models would underestimate in situ nitrification rates.

2. Materials and Methods

2.1. Study Site Description and Experimental Set Up

This study was conducted at the Gloucester Point Beach STE (GP-STE, 37.248,884°N, 76.505,324°W), which is located along the York River Estuary, a tributary of the Chesapeake Bay. The GP-STE is a well-studied system where groundwater discharge to overlying water has been observed (Beck et al., 2016; Luek & Beck, 2014; Wilson, Anderson, Song, & Tobias, 2023). It is a sandy sediment beach; approximately 30 m long with a rock jetty on either side and a tidal height of ∼0.8 m; a detailed site description can be found in (Beck et al., 2016). Annual average groundwater discharge at this site has been estimated as 38 ± 11 L m^{-2} d^{-1} by Wilson, Anderson, Song, and Tobias (2023) and 39–62 L m^{-2} d^{-1} by Beck et al. (2016). Groundwater in the GP-STE, below 200 cm, is NH_4^+ rich (>100 μM), but in the STE profile, where salinity increases, and surface and groundwater appear to be mixing, a NO_3^- (>50 μM) peak has been observed (Wilson, Anderson, Song, & Tobias, 2023). The porewater profiles suggest that NH_4^+-rich groundwater is advected upwards into the oxic portion of the STE nitrified to oxidized DIN (Wilson, Anderson, Song, & Tobias, 2023).

To estimate nitrification rates in the oxic portion (0–70 cm; Wilson, Anderson, Song, & Tobias, 2023) of the STE, three methods were employed: conservative mixing models, an in situ tracer experiment, and ex situ sediment slurry incubations. Conservative mixing models were constructed from in situ geochemical characteristics of STE porewater collected seasonally in 2018–2019 from dedicated piezometers (wells) installed at the GP-STE as described by Wilson, Anderson, Song, and Tobias (2023). An in situ tracer experiment was conducted at the site in 2019 in two wells, targeting 50 cm in the oxic zone (Figure S1 in Supporting Information S1). The ex situ sediment slurry incubations were conducted in 2020. Sediment cores were collected from the beach adjacent to the existing GP-STE wells, from which porewater (0 to 50 cm) was collected for addition to the slurries. Each measurement method is described in detail below.

2.2. Conservative Mixing Calculations

Porewater samples were collected in four seasons (2018–2019) from dedicated piezometers and analyzed for sample salinity and concentrations of NH_4^+ and NO_3^- as described by Wilson, Anderson, Song, and Tobias (2023). Profiles used here included samples taken every 10 cm from surface water (0) to 110 cm in the subsurface. The vertical salinity distribution was used to construct conservative two endmember derived mixing lines for NH_4^+ and NO_3^- extending from surface water (0) to 110 cm (10 piezometers and 1 surface sample per season) for each of the four seasons sampled. Conservatively mixed concentrations were calculated from the fractions of fresh and saltwater endmembers and their respective NH_4^+ and NO_3^- concentrations according to:

$$C_i = \left(f_{\mathrm{sw}-i} * C_{\mathrm{sw}}\right) + \left(f_{\mathrm{gw}-i} * C_{\mathrm{gw}}\right) \quad (1)$$

where C_i is the calculated concentration for a given depth interval, C_{sw} is the surface water endmember concentration, C_{gw} is the groundwater endmember concentration, $f_{sw\text{-}i}$ and $f_{gw\text{-}i}$ are the fractions of saline surface water and fresh groundwater, respectively calculated as:

$$f_{\mathrm{sw}-i} = (S_i - S_{\mathrm{gw}}) / (S_{\mathrm{sw}} - S_{\mathrm{gw}}) \quad (2)$$

where $f_{sw\text{-}i}$ is the fraction of saline surface water at a given depth in the STE, S_i is the salinity of porewater at that depth, S_{gw} is the salinity of the groundwater endmember, and S_{sw} is the salinity of the surface water endmember. The fraction of fresh groundwater ($f_{gw\text{-}i}$) at a given depth in the STE was determined as:

$$f_{\mathrm{gw}-i} = 1 - f_{\mathrm{sw}-i} \quad (3)$$

The observed concentrations of NH_4^+ and NO_3^- were compared to the predicted concentrations to determine subsidies or deficits in NH_4^+ and NO_3^- respectively along the STE salinity gradient. Similar to Santos et al. (2008), these data were determined to exhibit either linear mixing (conservative), removal, or production.

21698961, 2024, 6, Downloaded from https://agupubs.onlinelibrary.wiley.com/doi/10.1029/2023JG007876 by Viva Jmu Procurement Services, Wiley Online Library on [30/03/2025]. See the Terms and Conditions (https://onlinelibrary.wiley.com/terms-and-conditions) on Wiley Online Library for rules of use; OA articles are governed by the applicable Creative Commons License

Surface water (0 cm) and porewater samples (110 cm-depth) served as the surface water and groundwater endmembers, respectively. These represent the DIN concentrations and salinity of the water bodies directly above and below the top 100 cm of the STE, which encompasses the mixing zone of fresh groundwater and overlying saline water. The endmember concentrations were used to calculate the conservative mixing line, which represents the predicted analyte concentrations resulting from mixing of surface water (saline) and groundwater (fresh) alone. The disparity between the predicted, conservative concentrations and the observed concentrations represents the production or consumption of that analyte (Figure S2 in Supporting Information S1). The integrated mass of N in the NO_3^- subsidy and NH_4^+ deficit relative to conservative mixing was converted to a net nitrification rate as:

$$R_1 = \frac{1}{t}\int_{\text{low salinity}}^{\text{high salinity}} (C_r - C_s)\,\mathrm{dS} \tag{4}$$

where R_1 is the rate (μmoles L^{-1} d^{-1}), t is the STE residence time (46 days as determined for the GP-STE using radium isotopes by Beck et al. (2016)), C_r is the observed concentration (μmoles L^{-1}), C_s is the predicted concentration due to mixing alone (μmoles L^{-1}), and dS is the salinity change. The area between C_s and C_r is integrated, resulting in the amount of NH_4^+ removed or NO_3^- produced along the salinity gradient in μmoles L^{-1} d^{-1}. The rate is converted to per m^2 using the following equation:

$$R_2 = R_1 * (\Phi * D_{mix}) \tag{5}$$

where R_2 is the per area NH_4^+ loss or NO_3^- production rate along the STE salinity gradient (μmoles m^{-2} d^{-1}), R_1 is the loss rate (as determined by Equation 4, μmoles L^{-1} d^{-1}), Φ is the porosity of the GP-STE sediment (0.3) measured by O'Connor et al. (2018), and D_{mix} is the depth of the assumed mixing zone (0–100 cm) that encompasses the STE salinity gradient. This approach yields a per square meter rate that assumes a constant nitrification rate integrated over the top 100 cm. A constant porosity is assumed for the top 100 cm of the STE due to the limited variation observed in sediment bulk density with depth (Table S1 in Supporting Information S1).

2.3. In Situ Experiment With $^{15}NH_4^+$ Tracer Injection

The in situ $^{15}NH_4^+$ tracer experiment was conducted in the summer of 2019 in the surficial, oxic sediments of the GP-STE to directly measure nitrification (complete oxidation of NH_4^+ to NO_x) under field conditions. The experiment was conducted as a hybrid single/two well, modified push-pull tracer test similar to that described by Addy et al. (2002), but with $^{15}NH_4^+$ tracer as the substrate and $^{15}NO_3^-$ as the measured product of nitrification. Duplicate clusters of dedicated piezometers consisting of 2 cm screens (AMS Gas Vapor Tip) attached to FEP tubing (Versilon, Saint-Gobain) as described by Wilson, Anderson, Song, and Tobias (2023), were installed 3 m apart along the mid-tide line. Each well cluster included an injection well, installed at 50 cm, and monitoring wells above and below the injection site at 40–60 cm. The 50 cm depth was chosen because it represents the top of the STE mixing zone, where anoxic, NH_4^+ rich groundwater is mixing with oxic surface water, forming an interface that may support nitrification (Figure 2). The 50 cm also represents the middle of the depth range over which the conservative mixing estimates were made and corresponds to the depth of sediment collection used in the ex situ tests (next section). One meter in front of the injection well clusters, a target well was installed to a depth of 50 cm, with wells above and below at 40–60 cm, respectively. Measurements of dissolved oxygen (DO), salinity, pH, and porewater nutrient concentrations were made prior to the tracer injection to determine background site conditions.

To prepare for injection, 5 L of porewater was collected from the duplicate injection wells (50 cm) using an Alexis V3.0 peristaltic pump (Proactive Environmental Products) and gas impermeable tubing (MasterFlex C-Flex Ultra, Cole Parmer) to fill Flex foil bags that had previously been evacuated. Porewater was transported to the lab at in situ temperature in 10 L FlexFoil Sample Bags (SKC Inc.) where it was amended with ^{15}N-NH_4^+ (99 atm%, Cambridge Isotope Laboratories, Inc.) and 22 mL of 0.1% sulfur hexafluoride (SF_6, Scott Specialty Gases, Inc.) to final aqueous concentrations of 15 μM $^{15}NH_4^+$ and 15 μM SF_6 (Tobias et al., 2009). SF_6 is a potent greenhouse gas but was critical for tracer plume tracking in this experiment. The amount of SF_6 used in this experiment had the greenhouse gas equivalent of combusting 0.036 gallons of gasoline (US-EPA, 2015). The $^{15}NH_4^+$ tracer concentration was chosen to match previously measured NH_4^+ concentrations at this depth. The amended injectate was agitated for 12 hr at in situ temperature (27°C) using an orbital shaker to allow for equilibration of

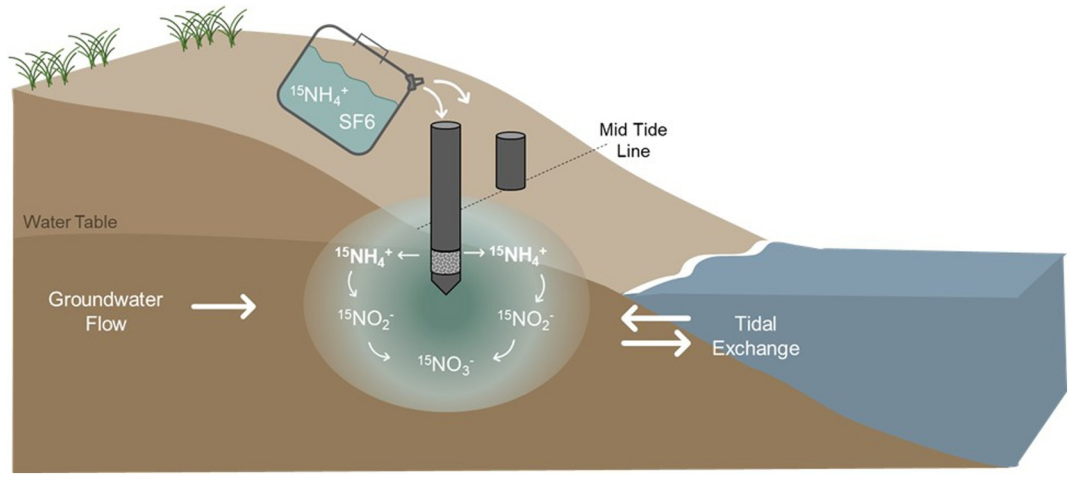

Figure 1. Conceptual diagram of in situ experiment showing the tracer plume introduction through the injection wells at the mid tide line into the mixing zone of groundwater and recirculated seawater in the subterranean estuarie and the potential oxidation of the tracer ($^{15}NH_4^+$) to $^{15}NO_2^-$ and $^{15}NO_3^-$ by nitrification.

the tracer amended porewater. After equilibration, the injectate was pumped back into the injection wells (50 cm) with a peristaltic pump at a rate of ~20 mL min^{-1} over four hours to minimize dispersion artifacts and to not artificially increase hydraulic head (Figure 1). Water samples were collected from the injectate bag and from the injection wells immediately following tracer addition and from injection and target wells were sampled roughly every 2 hr post injection then at regular time intervals over the following days informed by sample SF_6 concentrations. At each sampling time point, samples of porewater SF_6 and DIN were collected from the injection wells using a peristaltic pump (Proactive Environmental Products) and gas impermeable tubing (MasterFlex C-Flex Ultra, Cole Parmer). Samples for SF_6 were collected in 30 mL serum bottles and crimp-capped. The concentration of SF_6 in porewater was determined with a gas chromatograph fitted with an electron capture detector (GC-ECD, Shimadzu). Samples for DIN concentrations and isotopic composition were filtered with a 0.45 µm disposable groundwater filter capsule (Millipore Sigma) into 50 mL centrifuge tubes that were placed on ice, transported to the lab, and frozen until analysis.

2.4. Ex Situ Sediment Slurry Incubations With $^{15}NH_4^+$ Tracer Addition

Three replicate sediment cores (50 cm in length) were collected from the GP-STE in the summer of 2020. The cores were sectioned into 10 cm increments and homogenized. Porewater was collected at the same time as the cores from surface water (0 cm) and wells at 10, 20, 30, and 40 cm using an Alexis V3.0 peristaltic pump (Proactive Environmental Products). Sediment slurries consisting of 10 g homogenized sediment and 40 mL porewater from the same depth section were combined in 100 mL HDPE bottles and amended with 5 atom% 15 µM $^{15}NH_4^+$ (Cambridge Isotope), similar to that described by Damashek et al. (2016) and Santoro et al. (2013). Samples were incubated on a shaker table, in the dark, at in situ temperature, and under aerobic conditions for 0 (*T*0), 6 (*T*1), and 12 (*T*2) hours. After the incubation period, samples were spun down, porewater was decanted and filtered with a 0.45 µm syringe filter (Whatman GE) and were frozen (−20°C) until analysis.

2.5. Analytical Methods, Isotopic ^{15}N Analysis, and Rate Calculations

The concentrations of NO_3^-, NO_2^-, and NH_4^+ in all samples were determined with a Lachat autoanalyzer (Lachat Instruments, Lachat QuikChem FIA + 8,000, detection limits: 0.2 µM NO_3^- and NO_2^-, 0.36 µM NH_4^+). The isotopic composition of the $^{15}NO_x$ samples collected during the in situ and ex situ experiments was determined using a modified version of the bacterial denitrifier method (Sigman et al., 2001) at the University of Connecticut (UCONN) stable isotope lab. A culture of *Pseudomonas aureofaciens* reduced NO_x in collected samples to N_2O. The isotopic composition of the N_2O was measured with isotope-ratio mass spectrometry (IRMS) (Sigman et al., 2001). Calibrations included laboratory standards (USGS 34 and USGS IAEA-NO-3) with known $^{15}NO_3^-$ enrichments that were analyzed as samples; reduced using the *P. aureofaciens* culture to N_2O and analyzed with IRMS, to confirm method efficiency (Bohlke & Coplen, 1995; Bohlke et al., 1993; Brand et al., 2014).

21698961, 2024, 6, Downloaded from https://agupubs.onlinelibrary.wiley.com/doi/10.1029/2023JG007876 by Viva Jmu Procurement Services, Wiley Online Library on [30/03/2025]. See the Terms and Conditions (https://onlinelibrary.wiley.com/terms-and-conditions) on Wiley Online Library for rules of use; OA articles are governed by the applicable Creative Commons License

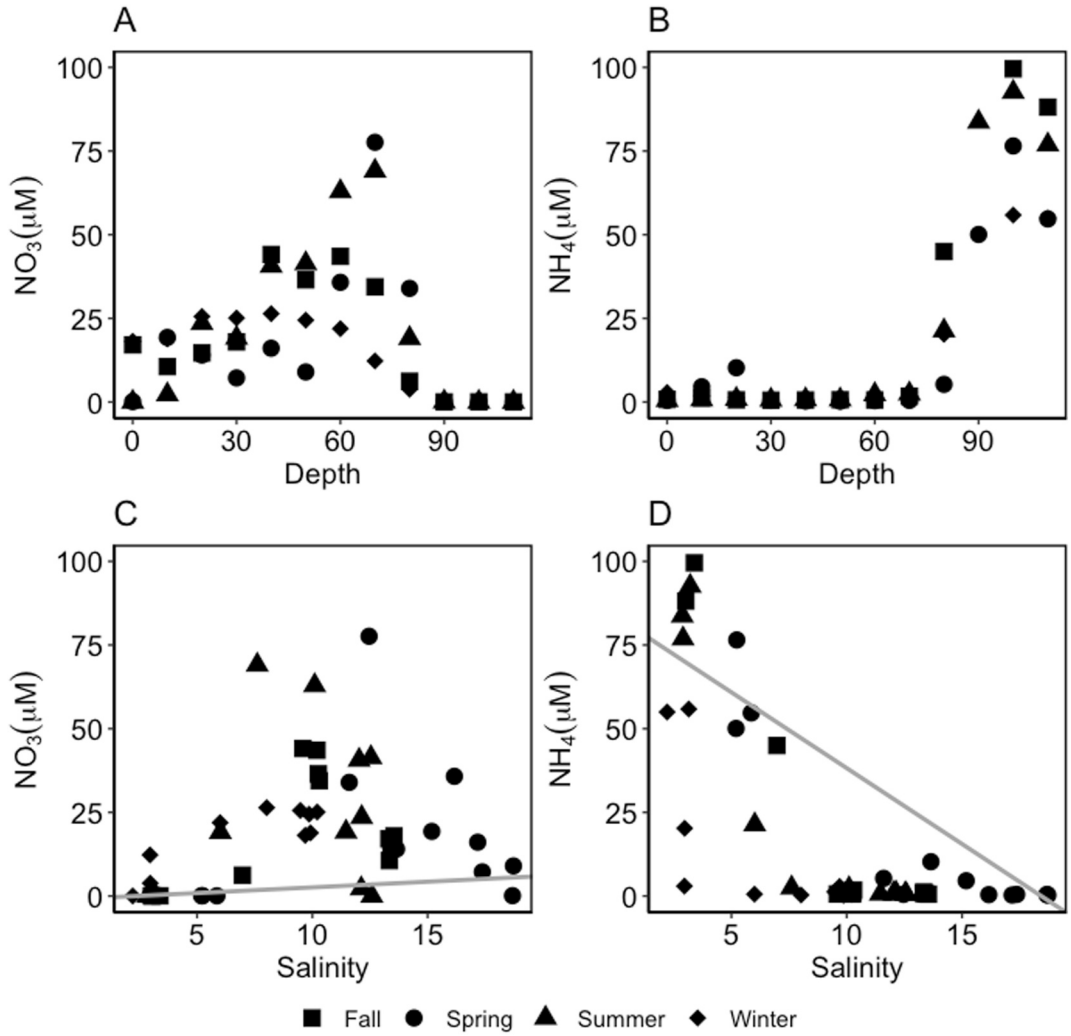

Figure 2. (a) Porewater NO_3^- concentrations (μM) in all seasons at each porewater sampling depth (cm); (b) porewater NH_4^+ concentrations (μM) in all seasons with porewater depth (cm); (c) porewater NO_3^- concentrations (μM) versus porewater salinity, with conservative mixing line (gray) for reference, (d) porewater NH_4^+ concentrations (μM) in all seasons indicated by point shape versus porewater Subterranean estuarie salinity, with the conservative mixing line (gray).

^{15}N composition for all data was reported in the delta notation, which was converted to ^{15}N mol fraction based on:

$$MF_{\text{sample}} = \frac{\left(\left(\frac{d15N_{\text{sample}}}{1000}+1\right) * \frac{15N_{ref}}{14N_{ref}}\right)}{1+\left(\left(\frac{d15N_{\text{sample}}}{1000}+1\right) * \frac{15N_{ref}}{14N_{ref}}\right)} \quad (6)$$

The excess ^{15}N mol fraction was calculated by subtracting the pre-tracer (background) $^{15}NO_x$ mole fraction from the measured $^{15}NO_x$ mole fraction in post tracer samples. The excess $^{15}NO_x$ mole fraction, multiplied by the measured concentration, yielded the ^{15}N mass in NO_x attributable to nitrification of the $^{15}NH_4^+$ as:

$$^{15}N\text{mass}_{\text{excess}} = MF_{\text{excess}} * C_{\text{sample}} \quad (7)$$

Rates of nitrification determined by the in situ tracer experiment were calculated as the change in the excess mass of $^{15}NO_x$ over time. The $^{15}NO_x$ mass was then corrected for the dilution of the $^{15}NH_4^+$ substrate over time resulting in, what is referred to here as, the nitrified N concentration over time. The evolving mole fraction of $^{15}NH_4^+$ was calculated based on proportional mixing of the 99 atom% tracer with NH_4^+ at 0 atom% enrichment.

21698961, 2024, 6, Downloaded from https://agupubs.onlinelibrary.wiley.com/doi/10.1029/2023JG007876 by Viva Jmu Procurement Services, Wiley Online Library on [30/03/2025]. See the Terms and Conditions (https://onlinelibrary.wiley.com/terms-and-conditions) on Wiley Online Library for rules of use; OA articles are governed by the applicable Creative Commons License

Table 1
STE Mixing Model Calculations of Production of NO_3^- and Consumption of NH_4^+ in the Top 100 cm of the STE in Each Season Sampled (Derived From 10 Piezometer and 1 Surface Sample per Season)

	Spring	Summer	Fall	Winter
NO_3^- production (μmol m^{-2} d^{-1})	147.30	177.99	106.79	39.67
NH_4^+ consumption (μmol m^{-2} d^{-1})	55.00	88.64	183.16	63.44

The proportion of each was calculated using the ratio of SF_6 measured in a sample to the SF_6 concentration in the injectate, C/C_0. Only samples from the core of the tracer plume were used for rate calculations; the core of the tracer plume is defined here as samples with a conservative tracer recovery (C/C_0 SF_6) > 0.05%, which included 68% of samples collected.

Nitrification rates as measured by the ex situ sediment slurry incubation were calculated as the change in the excess mass of $^{15}NO_x$ over time. The sediment slurry incubations are potential rate measurements (Hansen et al., 1981), because unlike the in situ approaches the slurries had oxygen in excess and ammonium concentrations were higher (~20 μM) than in situ throughout the incubation where added $^{15}NH_4^+$ was quickly diluted to near in situ concentrations (<5 μM). Rates were converted from a μmoles *g* of $sediment^{-1}$ d^{-1} rate to per areal rates in μmoles m^{-2} d^{-1} by multiplying the 10 cm increment the rate by the bulk density of that sediment depth increment (g cm^{-3}) and then converting from cm^2 to m^2.

3. Results

3.1. Nitrification Rates Estimated by Conservative Mixing Models

Spatial and temporal variations in GP-STE geochemical profiles are reported in detail in Wilson, Anderson, Song, and Tobias (2023). Briefly, NO_3^- concentrations were low (<10.0 μM) at depths deeper than 90 cm, whereas at the mid-salinity, mid-depth (40–90 cm) concentrations were much higher and, in some instances, exceeded 50 μM (Figure 2a). In contrast, NH_4^+ concentrations were >50 μM in groundwater deeper than 90 cm, but were <10.0 μM in surficial, higher salinity porewater (0–50 cm, Figure 2b). Groundwater NO_2^- concentrations were <0.50 μM. The NO_3^- and NH_4^+ mixing curves indicated two endmembers: groundwater and overlying surface water (Figures 2c and 2d). The observed NO_3^- concentrations were higher than the predicted, conservative values along the STE salinity gradient (Figure 2c). In contrast, observed porewater NH_4^+ concentrations were lower than predicted values determined by conservative mixing (Figure 2d).

The NO_3^- subsidies and NH_4^+ deficits in the GP-STE, as compared to the conservative mixing lines, were observed in all seasons (Figure S3 in Supporting Information S1). Nitrification rates in the top 100 cm of the STE were derived from net production and consumption of NO_3^- and NH_4^+, respectively. NO_3^- production in the top 1 m of the STE resulted in nitrification rates that ranged from 39.4 to 181 μmol N m^{-2} d^{-1} (Table 1). Rates of nitrification based on NH_4^+ consumption ranged from 53.5 to 84.7 μmol N m^{-2} d^{-1}. Seasonal variation was observed; the highest rate of NO_3^- production was observed in summer and the lowest in winter whereas the highest rate of NH_4^+ consumption was observed in fall and the lowest in spring.

3.2. Nitrification Rates Measured by an In Situ $^{15}NH_4^+$ Tracer Injection Experiment

In situ $^{15}NH_4^+$ tracer experiments were conducted to measure nitrification rates and determine the fate of *N* under field conditions. Injection sites (50 cm) were in the region of the STE where increasing NO_3^- concentrations and decreasing NH_4^+ concentrations were observed (Figures 2a and 2b). The 50 cm depth is oxic, brackish and within the groundwater-surface water mixing zone. Injection sites exhibited similar conditions with respect to porewater DO, salinity, pH, and DIN concentrations (Table 2) prior to tracer injections.

NH_4^+ concentrations in the injectates were 13.7–14.5 μM for injection well #1 and #2, respectively, within 10% of our target concentration. NH_4^+ concentrations decreased over time and were <5 μM an hour after injection, likely due to immediate dilution of the tracer plume by in situ ground/porewater. Concentrations of NH_4^+ ranged from 0.530 to 3.65 μM in all samples (Figures 3c and 3d). High frequency sampling of STE porewater during the tracer experiment revealed variance in NO_x concentrations overtime, but there was no clear pattern of NO_x production

Table 2
Background Geochemical Parameters at Injection Sites (50 cm Injection Wells) Prior to In Situ Tracer Experiment

	Depth (cm)	Salinity	DO (μM)	pH	Temp (°C)	NO_3^- (μM)	NH_4^+ (μM)
Inj. Site 1	50	13.85	145	6.78	26.97	121.67	0.73
Inj. Site 2	50	16.82	157	6.91	27.09	127.16	1.17

21698961, 2024, 6, Downloaded from https://agupubs.onlinelibrary.wiley.com/doi/10.1029/2023JG007876 by Viva Jmu Procurement Services, Wiley Online Library on [30/03/2025]. See the Terms and Conditions (https://onlinelibrary.wiley.com/terms-and-conditions) on Wiley Online Library for rules of use; OA articles are governed by the applicable Creative Commons License

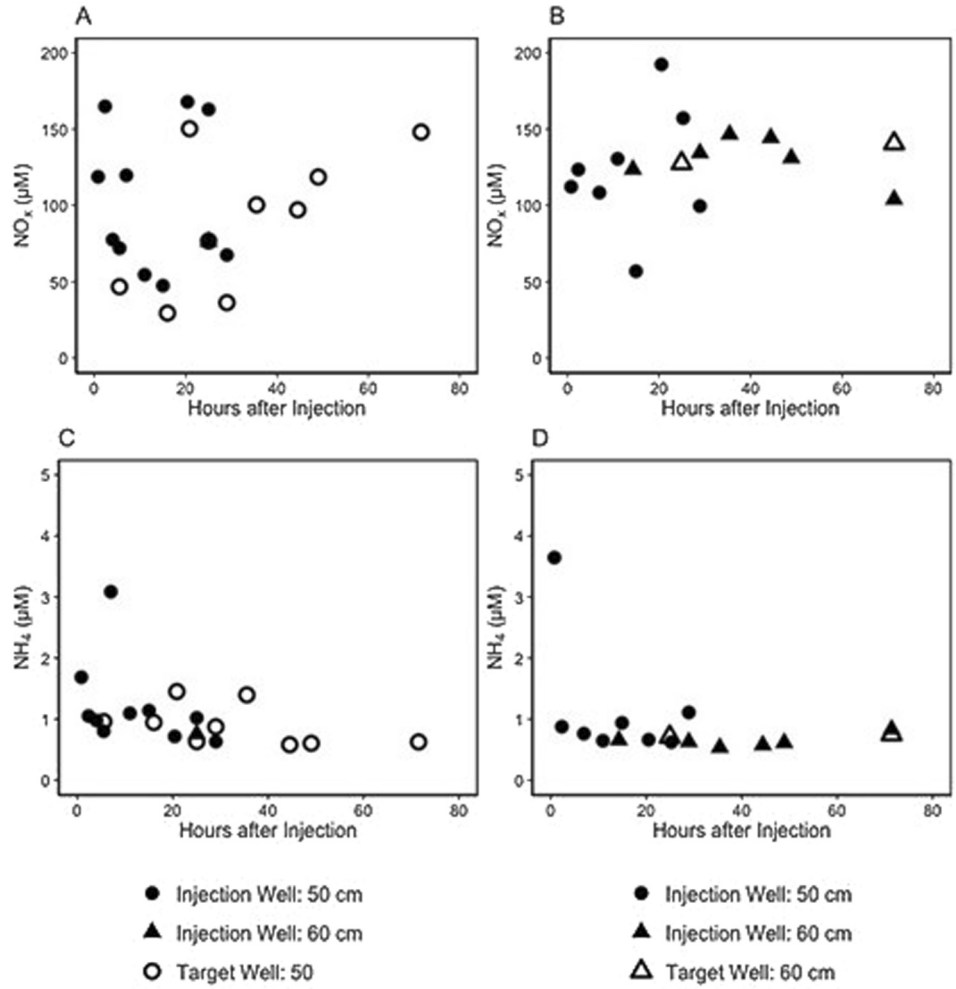

Figure 3. Groundwater NO_x^- concentrations (µM) over time after injection in the in situ tracer injections #1 (a) and #2 (b) and NH_4^+ concentrations (µM) in injections #1 (c) and #2 (d); well ID is indicated by point shape.

was detectable above background concentrations in injection wells (Figures 3a and 3b). The 50 cm target well at injection site #1 was the only well to exhibit an increase in NO_x overtime (Figure 3a), which could indicate nitrification. The concentrations of NO_x during the in situ experiment ranged from 47.4 to 192 µM and the NO_x pool was comprised primarily of NO_3^-; NO_2^- concentrations in all samples were <0.220 µM. Concentrations of the conservative tracer, SF_6, following tracer injection were initially >300 pM, but decreased over time resulting in concentrations of <100 pM SF_6 within 30 hr after injection (Figures 4a and 4b). Target wells consistently exhibited lower SF_6 concentrations as compared to injection wells as the plume was diluted during transport.

Despite no clear pattern in the concentrations of total NO_x in the injection wells during the experiment, the enrichment of ^{15}N in NO_x at both injection sites increased over time, indicating oxidation of the $^{15}NH_4$ tracer in the STE (Figures S4a and S4b in Supporting Information S1). The highest $^{15}NO_x$ enrichments were on the order of 6,900 d^{15}N which is approximately 2% of the in situ nitrate pool derived from nitrification of the added $^{15}NH_4^+$. Injection wells in both sites exhibited higher enrichments as compared to the target wells (Figures S4a and S4b in Supporting Information S1). The $^{15}NO_x$ delta values indicate a decrease in enrichment ~40 hr after injection, likely the result of dilution of the $^{15}NH_4^+$ tracer overtime. Dilution results from $^{14}NH_4^+$ produced by mineralization, and background $^{14}NH_4^+$ supplied by groundwater advection. When the isotope dilution of the $^{15}NH_4^+$ tracer is accounted for, the nitrified *N* produced over time is linear (Figures 5a and 5b, *p*-value <0.05). The in situ nitrification rates, based on this increase in $^{15}NO_x$ over time, were 7.50 ± 2.31–3.14 ± 0.51 µmol N L^{-1} d^{-1} in injection sites #1 and #2, respectively. These rates extrapolated to per m^2 become 225 ± 69.2–94.2 ± 15.2 µmol N m^{-2} d^{-1} in injection well #1 and #2, respectively.

21698961, 2024, 6, Downloaded from https://agupubs.onlinelibrary.wiley.com/doi/10.1029/2023JG007876 by Viva Jmu Procurement Services, Wiley Online Library on [30/03/2025]. See the Terms and Conditions (https://onlinelibrary.wiley.com/terms-and-conditions) on Wiley Online Library for rules of use; OA articles are governed by the applicable Creative Commons License

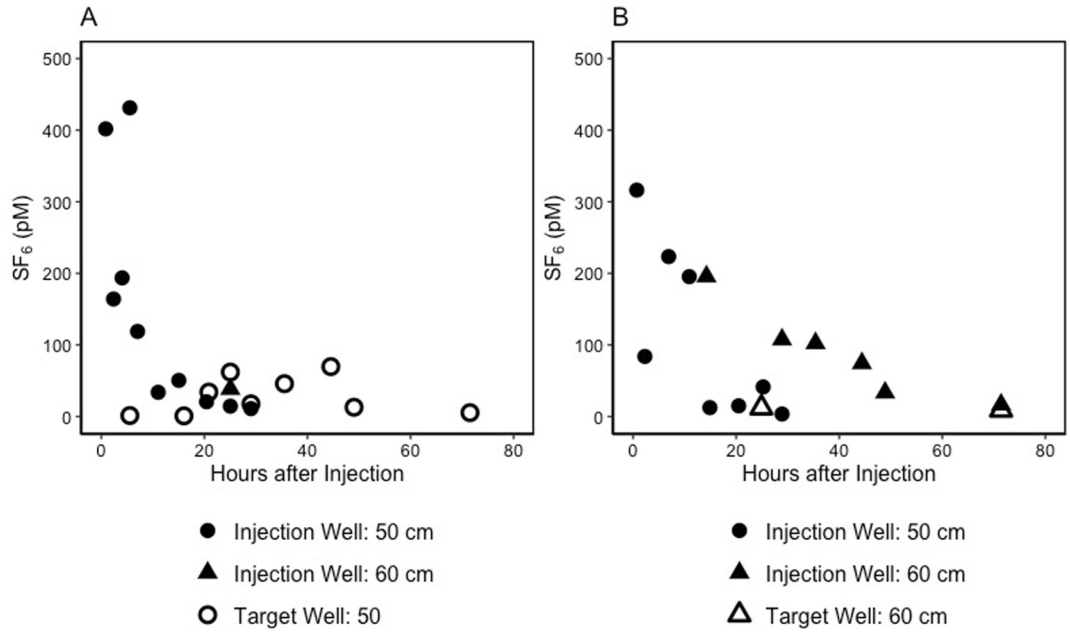

Figure 4. SF_6 concentrations (pM) in groundwater samples over time after the in situ tracer injections #1 (a) and #2 (b); sample well ID is indicated by point shape.

3.3. Nitrification Rates Measured in Ex Situ Sediment Slurry Incubations With Added $^{15}NH_4^+$ Tracer

Potential nitrification rates were measured in sediment slurries amended with $^{15}NH_4^+$ tracer. There was no clear pattern in the slurry NH_4^+ concentrations over time, which ranged from 18.4 to 29.1 μM (Figure S5 in Supporting Information S1). The NO_x pool was primarily comprised of NO_3^- and NO_2 concentrations were <0.24 μM. NO_x concentrations increased over time in all samples (Figure 6a) ranging from 1.86 to 24.4 μM. The concentration of enriched $^{15}NO_x$ also increased in all incubations, indicating oxidation of the $^{15}NH_4^+$ tracer to $^{15}NO_x$ (Figure 6b).

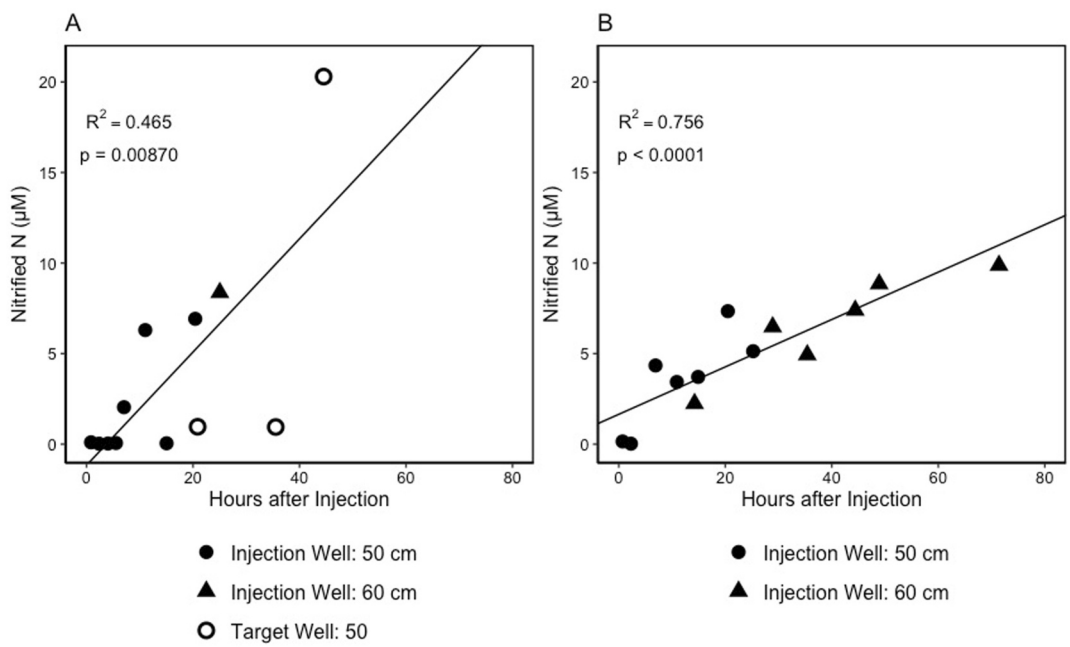

Figure 5. Nitrified N concentrations (μM; ^{15}NOx corrected for dilution of $^{15}NH4^+$ tracer) in groundwater samples after the in situ tracer injections #1 (a) and #2 (b). Where sampling well is indicated by point shape.

21698961, 2024, 6, Downloaded from https://agupubs.onlinelibrary.wiley.com/doi/10.1029/2023JG007876 by Viva Jmu Procurement Services, Wiley Online Library on [30/03/2025]. See the Terms and Conditions (https://onlinelibrary.wiley.com/terms-and-conditions) on Wiley Online Library for rules of use; OA articles are governed by the applicable Creative Commons License

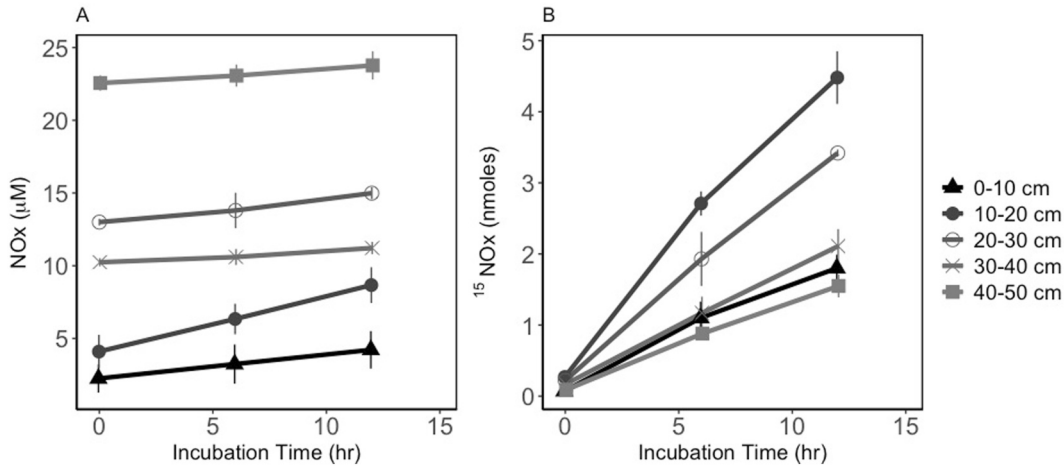

Figure 6. (a) NO_x concentrations (μM) overtime and (b) $^{15}NO_x$ (nmoles) overtime in sediment slurry incubations for each core depth section (indicated by point shape). Each point represents the mean of triplicate cores samples and error bars represent one standard error in each direction.

Potential nitrification rates ranged from 36.6 ± 3.68 to 109 ± 8.50 μmol N m^{-2} d^{-1} (Table 3). Rates varied with core depth section; the 10–20 cm core section exhibited the highest production rate, whereas the 30–40 cm core section had the lowest rate.

4. Discussion

4.1. Comparing Nitrification Rate Measurement Methods

In this study, all three methods indicated active nitrification, but the magnitude of the rates was dependent on the measurement method. Comparing the areal rates, the ex situ sediment slurries revealed higher rates than conservative mixing estimates and in situ tracer injections (Figure 7). In situ tracer rates were converted to areal rates over a depth of 20 cm which represents the oxic portion of profile and presumed zone of nitrification. Slurry rates were converted to area rates over a depth of 50 cm which also encompass the oxic profile and presumed zone of nitrification. Mixing model rates were converted to area rates by over the 100 cm of the STE bounded by clear endmembers for salinitiy, NO_3^-, and NH_4^+. This interval spans both oxic and variably hypoxic zones and thus includes both the zone of nitrification and likely deeper zones that are transiently hypoxic and may support nitrate reduction. It is important to recognize that the mixing model estimations describe net nitrification whereas the tracer injection and incubation experiment measure nitrification directly in the STE. However, by comparing the areal rates, the methods and their utility for understanding STE biogeochemical cycling may be assessed.

Mixing model calculations represent biogeochemical reactions over longer timescales than short term incubation or injection experiments. It is clear from this work and others (Santos et al., 2009; Wilson et al., 2024) that these calculations identify major biogeochemical processes occurring in STEs and the net effect over the salinity gradient, but our data suggest they may underestimate in situ rates. They represent a relatively simple way to estimate in situ rates from porewater profiles, particularly net rates integrated over timescales commensurate with water transit through the STE. Porewater profiles are widely available for many STEs, which can make these mixing calculations useful in comparing biogeochemical cycling across sites (Wilson et al., 2024) or in determining which processes may be important to measure directly. Therefore, mixing model calculations are useful for assessing the impact of STEs on coastal groundwater nutrient concentrations, especially when the resources for direct measurements are not available or site conditions make it difficult to conduct tracer tests.

Ex situ sediment slurry incubations do provide direct rate measurements, but microcosm incubations, such as slurries, have been reported to underestimate

Table 3
Benchtop Sediment Slurry Incubation Rates (±Standard Error) Determined by ^{15}N-NO_x Production Overtime in Incubation Samples

Depth section (cm)	Potential rate (μmoles m^{-2} d^{-1})
0–10	46.44 ± 5.28
10–20	109.02 ± 8.50
20–30	71.50 ± 1.18
30–40	48.68 ± 5.43
40–50	36.57 ± 3.68

Note. The average potential nitrification rate (all measurements) was 62.44 ± 7.23.

21698961, 2024, 6, Downloaded from https://agupubs.onlinelibrary.wiley.com/doi/10.1029/2023JG007876 by Viva Jmu Procurement Services, Wiley Online Library on [30/03/2025]. See the Terms and Conditions (https://onlinelibrary.wiley.com/terms-and-conditions) on Wiley Online Library for rules of use; OA articles are governed by the applicable Creative Commons License

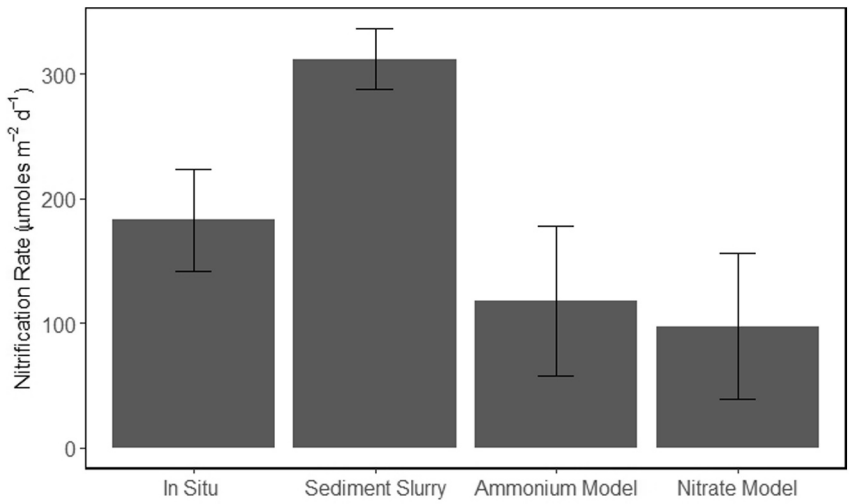

Figure 7. Comparison of average nitrification rates (μmoles N m^{-2} d^{-1}) as determined by the in situ tracer experiment (average of both injection sites, $n = 2$), sediment slurry incubation (summed across depth sections, $n = 3$), and conservative mixing models of ammonium loss and nitrate production (sum of mass from 0 to 100 cm; averaged across seasons, $n = 4$). Error bars represent one standard error in each direction.

(Addy et al., 2002) or overestimate (Riekenberg et al., 2017) rates. Major criticisms of slurry incubations include the disruption of sediment structure, microsites, and geochemical gradients, such as oxic-anoxic boundaries. Taking sediments out of their in situ environment can also introduce oxygen, which can be especially problematic for anoxic sediments and could result in a priming effect. In the GP-STE system, surficial sediments are oxygenated, which supports the use of oxic slurries, and the ^{15}N-tracer method used here. However, in an advective system like an STE, removal of samples and creating slurries homogenizes microscale heterogeneity and isolates the samples from groundwater flow which may supply reactants and remove products at the reaction site. Many of these artifacts associated with sample removal, homogenization, and incubation in the lab can also lead to shifts in microbial community structure and function that could affect rates (Riekenberg et al., 2017). Despite these caveats, laboratory incubations can test for factors that influence biogeochemical processes in a controlled setting. This can provide crucial information about mechanisms controlling STE processes. Our data suggest that sediment slurries are useful tests, but because they detach processes from the complex biogeochemistry and variable physical characteristics of the subsurface environment, they may not reflect in situ rates.

In contrast to the conservative mixing calculations or sediment slurry incubations, in situ tracer experiments maintain the field environment. Despite minor potential disruptions to substrate concentrations and hydraulic gradients (Smith et al., 2006) during tracer injection, which are minimized, when possible, these experiments allow for in situ flow, heterogeneity, and conditions. The in situ tracer method maintains connectivity to NH_4^+ supplied to the reaction site and heterogeneity that could present reactive microsites. These factors may also explain why rates measured in replicate injection sites exhibited high spatial variation. More specifically, spatial variability might be driven by differences in geochemical gradients, tidal pumping, and groundwater advection across the beach (Robinson et al., 2018). This variation was not reflected in rates derived from slurry incubations or conservative mixing calculations. It is difficult, if not impossible, to replicate the complicated and variable conditions of STEs, which are influenced by a range of abiotic and biotic factors (Russoniello et al., 2016; Slomp & Cappellen, 2004). In situ studies are highly sensitive, include small-scale heterogeneities, do not isolate processes from other subsurface reactions, and hydraulic gradients which may impact reaction rates remain unchanged (Bohlke et al., 2006; Jiang et al., 2023). The in situ tracer method is complex but is likely the best available method for measuring rates in groundwater systems. That being said, as in situ experiments are not always practical, conservative mixing models and incubations can provide useful information about STE biogeochemistry, variation in process rates across space and time, and define drivers of process rates relevant for determining the impact of SGD nutrient loading.

21698961, 2024, 6, Downloaded from https://agupubs.onlinelibrary.wiley.com/doi/10.1029/2023JG007876 by Viva Jmu Procurement Services, Wiley Online Library on [30/03/2025]. See the Terms and Conditions (https://onlinelibrary.wiley.com/terms-and-conditions) on Wiley Online Library for rules of use; OA articles are governed by the applicable Creative Commons License

21698961, 2024, 6, Downloaded from https://agupubs.onlinelibrary.wiley.com/doi/10.1029/2023JG007876 by Viva Jmu Procurement Services, Wiley Online Library on [30/03/2025]. See the Terms and Conditions (https://onlinelibrary.wiley.com/terms-and-conditions) on Wiley Online Library for rules of use; OA articles are governed by the applicable Creative Commons License

4.2. Mixing Model Calculations

Both consumption (NH_4^+) and production (NO_3^-) were used to determine nitrification rates from mixing model calculations. Rates determined from NO_3^- production were, when averaged across seasons, higher than those estimated from NH_4^+ consumption. The disparity between the NO_3^- and NH_4^+ based rates may be the result of exchange of NH_4^+ with the sorbed phase as NH_4^+ is oxidized, thereby dampening the apparent loss of NH_4^+ to nitrification. This approach integrates over a 46 days period across zones in the STE supportive of both nitrification and denitrification. The timescale of this integration is ∼15 times longer than the duration of the tracer test. It is likely that some of nitrate produced via nitrification is denitrified either due to changing redox conditions or the diffusion of nitrification products into anoxic regions or miscrosites in the STE. When evaluated over the duration of the water residence time this approach yields net nitrification rates which are lower than the rates measured by the tracer test which was confined to the nitrifying zone. We suggest this mechanism as the reason why, although both methods are in situ, the tracer test yields higher rates.

Inherent assumptions of conservative mixing calculations present limitations of these estimations. For example, we assume homogeneous mixing, which in this study, would be mixing in the top 100 cm of the STE. Vertical profiles of salinity and DO (Wilson, Anderson, Song, & Tobias, 2023) suggest mixing of groundwater and surface water. Previous measurements of hydraulic gradients and groundwater seepage indicate vertical groundwater flow in the top 100 cm of the STE and, therefore, mixing (Beck et al., 2016; Wilson, Anderson, Song, & Tobias, 2023). However, varying hydraulic conductivities in sediment layers (Ullman et al., 2003), fissures, or bioturbation can complicate subsurface flow paths (Shrivastava et al., 2021). It is important to recognize that sediments and flow paths are heterogeneous, so homogeneity of mixing in the subsurface environment is unlikely, but flow toward overlying water is observed at this site. Sediment heterogeneity can influence groundwater residence times, another crucial term in conservative mixing model estimates. Here the residence time estimated with radium isotopes (Beck et al., 2016) for the GP-STE, but it is likely that this residence time varies across different reaction zones, with spring-neap tidal cycles, seasons, and hydrologic conditions (Slomp & Cappellen, 2004). The variation in residence time may be better constrained with long term monitoring of hydraulic gradients. Endmember concentrations are also critical to conservative mixing models as they are used to calculate the conservative mixing line. At this site, significant variation in the DIN concentrations across space and tidal stage was not observed, but there were significant changes across seasons (Wilson, Anderson, Song, & Tobias, 2023). This suggests that, at this site and in this study, endmembers may be stable over the modeled scale (seasonally); however, STEs are highly variable, and this may not hold true across locations. Substantial site characterization to verify that the assumptions of conservative mixing are required to ensure reasonable outputs.

4.3. In Situ Tracer Experiment

To measure nitrification and determine the fate of N under in situ conditions, a $^{15}NH_4^+$ was injected into the STE. The conservative tracer (SF_6) data indicated that the tracer plume was constrained within the 40–60 cm depth range of the STE and, therefore, our resulting rates are averaged across this depth interval. Dilution of the tracer plume, including both SF_6 and $^{15}NH_4^+$ concentrations, over time was likely driven by tidal pumping, an important factor controlling STE biogeochemistry (Moosdorf et al., 2021; Robinson et al., 2018; Rocha et al., 2021; Slomp & Cappellen, 2004), and groundwater advection. Overlying water and groundwater outside the tracer plume have no SF_6, so as this water mixes with the plume, the concentrations of SF_6 decrease. This is similar for $^{15}NH_4^+$ as there will be essentially no isotopic enrichment of organic matter or NH_4^+ in overlying water and groundwater, so as NH_4^+ is produced via remineralization of organic matter or supplied by groundwater advection, the $^{15}NH_4^+$ in the tracer plume is diluted.

Active nitrification in the STE was revealed by $^{15}N\text{-}NO_x$ production at both injection sites overtime (Figures 7a and 7b). Although both injection sites were the same depth (50 cm) and had similar background geochemical conditions, they exhibited different nitrification rates. The variation in the observed rates between wells is likely due to STE heterogeneity in physical, chemical, and biological conditions at the flowpath scale. Previous work at this site has shown gradients in nutrient concentrations, salinity, and DO on the order of 10 cm, that there are vertical migrations of these profiles seasonally, and that hydraulic gradients vary over tidal cycles (Wilson, Anderson, Song, & Tobias, 2023). Therefore, despite being only a few meters apart, there may be transient redox oscillations, distinctive microbial community structure, or a higher abundance of nitrifiers between injections due to STE variability. Hydraulic gradients and groundwater flow-paths combined with tidal pumping can also vary

21698961, 2024, 6, Downloaded from https://agupubs.onlinelibrary.wiley.com/doi/10.1029/2023JG007876 by Viva Jmu Procurement Services, Wiley Online Library on [30/03/2025]. See the Terms and Conditions (https://onlinelibrary.wiley.com/terms-and-conditions) on Wiley Online Library for rules of use; OA articles are governed by the applicable Creative Commons License

across small spatial scales (Slomp & Cappellen, 2004; Smith et al., 2015), influencing the transport of analytes, such as NH_4^+ and DO. The in situ experiment, and the subsurface variability it revealed, supports the known complexity of STE systems and the importance of using in situ measurements to define a range of possible rates under ambient conditions.

Similar in situ tracer approaches have been used to measure denitrification (Addy et al., 2002; Smith et al., 2015) and nitrification (Böhlke et al., 2006; Smith et al., 2006) in groundwater systems. Smith et al. (2006) used in situ tracer injections to measure anoxic nitrification rates in a Cape Cod, MA, USA aquifer and observed rates (0.480–6.72 μmol L^{-1} d^{-1}), which were comparable to those measured in the GP-STE (3.14–7.50 μmol L^{-1} d^{-1}). The STE is within the intertidal zone, where mixing of fresh and saltwater as well as complex subsurface flow paths can create biogeochemical dynamics that may stimulate reaction rates. In this way, the STE is similar to hyporheic zones, where particle and solute transport can stimulate biogeochemical reactions (Harvey et al., 2012). Both STEs and the hyporheic zones can support high biogeochemical reaction rates as organic matter and oxygen supplied by surface waters meets anoxic, nutrient rich groundwater within complex, subsurface flow paths (Krause et al., 2011; Moore, 1999).

4.4. Ex Situ Sediment Slurry Incubation Experiments

Potential nitrification rates were also measured in sediment slurry incubations amended with $^{15}NH_4^+$. Nitrification was evidenced by the increase in the $^{15}NO_x$ concentrations over time and rates varied with depth section. Variation in nitrification rates may be driven by nitrifier abundance, activity, or background NH_4^+ concentrations. Nitrifying prokaryotes have been identified in the GP-STE, revealing genetic potential for nitrification (Wilson, Anderson, & Song, 2023); however, sediment slurry rates did not correlate with reported nitrifier abundance. These studies were not conducted in tandem, so the abundances previously measured may not represent those in the present samples and the presence of nitrifiers, does not necessarily directly relate to activity. Nitrification rates were, however, related to background porewater NH_4^+ concentrations ($R^2 = 0.33$, Figure S6 in Supporting Information S1); samples with the highest rates also had the highest porewater ammonium concentrations prior to the incubation. This suggests a link between available substrate (NH_4^+) and potential process rates.

Potential nitrification rates were on an order of magnitude lower in the GP-STE (0.366–1.09 μmol L^{-1} d^{-1}) than those measured with potential slurry incubations in a sandy beach system on Sapelo Island, GA, USA (23.5 ± 3.60 μmol L^{-1} d^{-1}) by Schutte et al. (2017). When compared to rates measured in coastal sediments of Japan (Usui et al., 2001) and California, USA (Wankel et al., 2011) the GP-STE rates were lower. Our observed rates (36.6–109 μmol m^{-2} d^{-1}) were within the reported rates compiled by Fennel et al. (2009) for aquatic sediments but were an order of magnitude lower than the average (1,860 μmol m^{-2} d^{-1}; Fennel et al., 2009). It was suggested by Schutte et al. (2017) that oxygen penetration into the subsurface drove nitrification rates and likely played a role in organic matter remineralization. Nitrification in the surficial 50 cm of the GP-STE is not oxygen limited as concentrations are >3.5 mg L^{-1} throughout the year and NH_4^+ could be supplied by both the nutrient-rich groundwater and remineralization of dissolved organic matter in recirculated surface water (Wilson, Anderson, Song, & Tobias, 2023), therefore, it is unlikely that oxygen scarcity is driving low rates compared to other sites. Alternatively, it is possible that the observed low rates may be the result of low NH_4^+ supply. The GP-STE sediments have low organic content (Wilson, Anderson, Song, & Tobias, 2023) and NH_4^+ delivery to the oxic zone by groundwater advection may be slow.

4.5. Implications for N in STEs

The nitrification rates determined in this study were lower than those measured in other coastal sediments from Monterey Bay estuary, CA, USA (Wankel et al., 2011), the Tama Estuary, Japan (Usui et al., 2001), and Sapelo Island, GA, USA (Schutte et al., 2017). The GP-STE rates were more like those observed in aquifers such as those reported in Cape Cod, MA, USA (Böhlke et al., 2006; Smith et al., 2006). Despite low nitrification rates observed in this system, the transformation of N has important implications for the release of nutrients in SGD to the coastal ocean. Many SGD studies assume conservative transport of nutrients when calculating fluxes (Brooks et al., 2021; Robinson et al., 2018). This assumption overlooks biogeochemical processing in the STE, assuming no transformation or removal along the flow path, which may inaccurately represent fluxes (Wilson, Anderson, Song, & Tobias, 2023). At this site, assuming conservative transport is reasonable as DIN in groundwater appears to be available as DIN to be discharged to overlying water. However, assuming conservative transport would not

incorporate the change from NH_4^+ to NO_x and would likely overestimate nutrient loading by SGD. Despite wide acceptance that assuming conservative transport is not representative of SGD fluxes, there remain few studies that measure and incorporate reaction rates into flux estimations. Here we compared three methods, which may be applied to STEs to estimate nitrification rates and although the magnitude of the rate was dependent on methodology, all estimates reflected active nitrification. Our data suggest that incubation experiments may over estimate in situ rates and mixing models may underestimate; however, the net effect of the STE may determined by any of these methods. N is limiting in many coastal estuaries, and SGD may contribute to or exacerbate eutrophication resulting from excess nutrient inputs across the land-ocean continuum (Howarth, 2008). To accurately assess nutrient export via SGD and the impact of groundwater derived nutrients on coastal ecosystems, it is critical to evaluate STE process rates and the consequences of those transformations for SGD fluxes.

Data Availability Statement

The geochemical profiles (https://www.bco-dmo.org/dataset/807664), ex situ incubation data (https://www.bco-dmo.org/dataset/915302), and in situ tracer data (https://www.bco-dmo.org/dataset/917767) described in this study are available on the BCO-DMO repository. Other data associated with this site and the larger project can be found via: https://www.bco-dmo.org/project/805722.

Acknowledgments

We would like to thank the Virginia Institute of Marine Science and the University of Connecticut for their support and resources. We also acknowledge funding for this work from the National Science Foundation (1658135 and 1737258). We thank Michele Cochran, Hunter Walker, Peter Ruffino, and Clare Schlink for technical assistance in the field and laboratory. We thank Dr. Julie Granger and the Granger lab for maintaining cultures of *Pseudomonas aureofaciens* utilized prepare samples for analysis in the stable isotope lab at the University of Connecticut.

References

Abarca, E., Karam, H., Hemond, H. F., & Harvey, C. F. (2013). Transient groundwater dynamics in a coastal aquifer: The effects of tides, the lunar cycle, and the beach profile. *Water Resources Research*, *49*(5), 2473–2488. https://doi.org/10.1002/wrcr.20075

Addy, K., Kellogg, D. Q., Gold, A. J., Groffman, P. M., Ferendo, G., & Sawyer, C. (2002). In situ push–pull method to determine ground water denitrification in riparian zones. *Journal of Environmental Quality*, *31*(3), 1017–1024. https://doi.org/10.2134/jeq2002.1017

Anschutz, P., Charbonnier, C., Deborde, J., Deirmendjian, L., Poirier, D., Mouret, A., et al. (2016). Terrestrial groundwater and nutrient discharge along the 240-km-long Aquitanian coast. *Marine Chemistry*, *185*, 38–47. https://doi.org/10.1016/j.marchem.2016.04.002

Beck, A. J., Kellum, A. A., Luek, J. L., & Cochran, M. A. (2016). Chemical flux associated with spatially and temporally variable submarine groundwater discharge, and chemical modification in the subterranean estuary at Gloucester point, VA (USA). *Estuaries and Coasts*, *39*, 1–12. https://doi.org/10.1007/s12237-015-9972-0

Beck, M., Reckhardt, A., Amelsberg, J., Bartholomä, A., Brumsack, H. J., Cypionka, H., et al. (2017). The drivers of biogeochemistry in beach ecosystems: A cross-shore transect from the dunes to the low-water line. *Marine Chemistry*, *190*, 35–50. https://doi.org/10.1016/j.marchem.2017.01.001

Bohlke, J. K., & Coplen, T. B. (1995). Interlaboratory comparison of reference materials for nitrogen-isotope-ratio measurements.

Bohlke, J. K., Gwinn, C. J., & Coplen, T. B. (1993). New reference materials for nitrogen-isotope-ratio measurements. *Geostandards Newsletter*, *17*(1), 159–164. https://doi.org/10.1111/j.1751-908x.1993.tb00131.x

Böhlke, J. K., Smith, R. L., & Miller, D. N. (2006). Ammonium transport and reaction in contaminated groundwater: Application of isotope tracers and isotope fractionation studies. *Water Resources Research*, *42*(5), 1–19. https://doi.org/10.1029/2005WR004349

Boyle, E., Collier, R., Dengler, A. T., Edmond, J. M., Ng, A. C., & Stallard, R. F. (1974). On the chemical mass-balance in estuaries. *Geochimica et Cosmochimica Acta*, *38*(11), 1719–1728. https://doi.org/10.1016/0016-7037(74)90188-4

Brand, W. A., Coplen, T. B., Vogl, J., Rosner, M., & Prohaska, T. (2014). Assessment of international reference materials for isotope-ratio analysis (IUPAC Technical Report). *Pure and Applied Chemistry*, *86*(3), 425–467. https://doi.org/10.1515/pac-2013-1023

Brooks, T. W., Kroeger, K. D., Michael, H. A., & York, J. K. (2021). Oxygen-controlled recirculating seepage meter reveals extent of nitrogen transformation in discharging coastal groundwater at the aquifer–estuary interface. *Limnology & Oceanography*, *66*(8), 3055–3069. https://doi.org/10.1002/lno.11858

Cho, H. M., Kim, G., Kwon, E. Y., Moosdorf, N., Garcia-Orellana, J., & Santos, I. R. (2018). Radium tracing nutrient inputs through submarine groundwater discharge in the global ocean. *Scientific Reports*, *8*, 1–7. https://doi.org/10.1038/s41598-018-20806-2

Cole, J. J., Peierls, B. L., Caraco, N. F., & Pace, M. L. (1993). Nitrogen loading of rivers as a human-driven process. In *Humans as components of ecosystems* (pp. 141–157). Springer.

Cole, M. L., Kroeger, K. D., McClelland, J. W., & Valiela, I. (2006). Effects of watershed land use on nitrogen concentrations and δ^{15} nitrogen in groundwater. *Biogeochemistry*, *77*(2), 199–215. https://doi.org/10.1007/s10533-005-1036-2

Couturier, M., Tommi-Morin, G., Sirois, M., Rao, A., Nozais, C., & Chaillou, G. (2017). Nitrogen transformations along a shallow subterranean estuary. *Biogeosciences*, *14*(13), 3321–3336. https://doi.org/10.5194/bg-14-3321-2017

Damashek, J., Casciotti, K. L., & Francis, C. A. (2016). Variable nitrification rates across environmental gradients in turbid, nutrient-rich estuary waters of San Francisco Bay. *Estuaries and Coasts*, *39*(4), 1050–1071. https://doi.org/10.1007/s12237-016-0071-7

Enoksson, V. (1986). Nitrification rates in the Baltic sea: Comparison of three isotope techniques. *Applied and Environmental Microbiology*, *51*(2), 244–250. https://doi.org/10.1128/aem.51.2.244-250.1986

EPA, U. S. (2015). Greenhouse gas equivalencies calculator. In *Greenhouse gas equivalencies calculator*. Retrieved from https://www.epa.gov/energy/greenhouse-gas-equivalencies-calculator

Erler, D. V., Santos, I. R., Zhang, Y., Tait, D. R., Befus, K. M., Hidden, A., et al. (2014). Nitrogen transformations within a tropical subterranean estuary. *Marine Chemistry*, *164*, 38–47. https://doi.org/10.1016/j.marchem.2014.05.008

Fennel, K., Brady, D., DiToro, D., Fulweiler, R. W., Gardner, W. S., Giblin, A., et al. (2009). Modeling denitrification in aquatic sediments. *Biogeochemistry*, *93*(1–2), 159–178. https://doi.org/10.1007/s10533-008-9270-z

Hansen, J. I., Henriksen, K., & Blackburn, T. H. (1981). Seasonal distribution of nitrifying bacteria and rates of nitrification in coastal marine sediments. *Microbial Ecology*, *7*(4), 297–304. https://doi.org/10.1007/BF02341424

21698961, 2024, 6, Downloaded from https://agupubs.onlinelibrary.wiley.com/doi/10.1029/2023JG007876 by Viva Jmu Procurement Services, Wiley Online Library on [30/03/2025]. See the Terms and Conditions (https://onlinelibrary.wiley.com/terms-and-conditions) on Wiley Online Library for rules of use; OA articles are governed by the applicable Creative Commons License

Harvey, J. W., Drummond, J. D., Martin, R. L., McPhillips, L. E., Packman, A. I., Jerolmack, D. J., et al. (2012). Hydrogeomorphology of the hyporheic zone: Stream solute and fine particle interactions with a dynamic streambed. *Journal of Geophysical Research*, *117*(4), G00N11. https://doi.org/10.1029/2012JG002043

Heiss, J. W., & Michael, H. A. (2014). Saltwater-freshwater mixing dynamics in a sandy beach aquifer over tidal, spring-neap, and seasonal cycles. *Water Resources Research*, *50*(8), 6747–6766. https://doi.org/10.1002/2014WR015574

Howarth, R. W. (2008). Coastal nitrogen pollution: A review of sources and trends globally and regionally. *Harmful Algae*, *8*(1), 14–20. https://doi.org/10.1016/j.hal.2008.08.015

Jäntti, H., Leskinen, E., Stange, C. F., & Hietanen, S. (2012). Measuring nitrification in sediments -comparison of two techniques and three $^{15}NO_3^-$ measurement methods. *Isotopes in Environmental and Health Studies*, *48*(2), 313–326. https://doi.org/10.1080/10256016.2012.641543

Jiang, S., Jin, J., Wei, Y., Wu, Y., Zhang, Y., Rocha, C., et al. (2023). Sandy seepage faces as bioactive nitrate reactors: Biogeochemistry, microbial ecology and metagenomics. *Geoscience Frontiers*, *14*(3), 101529. https://doi.org/10.1016/j.gsf.2022.101529

Krause, S., Hannah, D. M., Fleckenstein, J. H., Heppell, C. M., Kaeser, D., Pickup, R., et al. (2011). Inter-disciplinary perspectives on processes in the hyporheic zone. *Ecohydrology*, *4*, 481–499. https://doi.org/10.1002/eco.176

Kroeger, K. D., & Charette, M. A. (2008). Nitrogen biogeochemistry of submarine groundwater discharge. *Limnology & Oceanography*, *53*(3), 1025–1039. https://doi.org/10.4319/lo.2008.53.3.1025

Lisa, J. A., Song, B., Tobias, C. R., & Hines, D. E. (2015). Genetic and biogeochemical investigation of sedimentary nitrogen cycling communities responding to tidal and seasonal dynamics in Cape Fear River Estuary. *Estuarine, Coastal and Shelf Science*, *167*, A313–A323. https://doi.org/10.1016/j.ecss.2015.09.008

Luek, J. L., & Beck, A. J. (2014). Radium budget of the York River estuary (VA, USA) dominated by submarine groundwater discharge with a seasonally variable groundwater end-member. *Marine Chemistry*, *165*, 55–65. https://doi.org/10.1016/j.marchem.2014.08.001

Moore, W. S. (1999). The subterranean estuary: A reaction zone of ground water and sea water. In *Marine chemistry* (Vol. 65(1–2), pp. 111–125). https://doi.org/10.1016/S0304-4203(99)00014-6

Moore, W. S. (2009). The effect of submarine groundwater discharge on the ocean. *Annual Review of Marine Science*, *2*(1), 59–88. https://doi.org/10.1146/annurev-marine-120308-081019

Moosdorf, N., Böttcher, M. E., Adyasari, D., Erkul, E., Gilfedder, B. S., Greskowiak, J., et al. (2021). A state-of-the-art perspective on the characterization of subterranean estuaries at the regional scale. *Frontiers of Earth Science in China*, *9*, 601293. https://doi.org/10.3389/feart.2021.601293

Nixon, S. W. (1995). Coastal marine eutrophication: A definition, social causes, and future concerns. *Ophelia*, *41*(1), 199–219. https://doi.org/10.1080/00785236.1995.10422044

O'Connor, A. E., Krask, J. L., Canuel, E. A., & Beck, A. J. (2018). Seasonality of major redox constituents in a shallow subterranean estuary. *Geochimica et Cosmochimica Acta*, *224*, 344–361. https://doi.org/10.1016/j.gca.2017.10.013

Officer, C. B., & Lynch, D. R. (1981). Dynamics of mixing in estuaries. *Estuarine, Coastal and Shelf Science*, *12*(5), 525–533. https://doi.org/10.1016/s0302-3524(81)80079-5

Riekenberg, P. M., Oakes, J. M., & Eyre, B. D. (2017). Uptake of dissolved organic and inorganic nitrogen in microalgae-dominated sediment: Comparing dark and light in situ and ex situ additions of ^{15}N. *Marine Ecology Progress Series*, *571*, 29–42. https://doi.org/10.3354/meps12127

Robinson, C., Xin, P., Li, L., & Barry, D. A. (2014). Groundwater flow and salt transport in a subterranean estuary driven by intensified wave conditions. *Water Resources Research*, *50*, 1–17. https://doi.org/10.1002/2013WR013813

Robinson, C. E., Xin, P., Santos, I. R., Charette, M. A., Li, L., & Barry, D. A. (2018). Groundwater dynamics in subterranean estuaries of coastal unconfined aquifers: Controls on submarine groundwater discharge and chemical inputs to the ocean. *Advances in Water Resources*, *115*, 315–331. https://doi.org/10.1016/j.advwatres.2017.10.041

Rocha, C., Robinson, C. E., Santos, I. R., Waska, H., Michael, H. A., & Bokuniewicz, H. J. (2021). A place for subterranean estuaries in the coastal zone. *Estuarine, Coastal and Shelf Science*, *250*, 107167. https://doi.org/10.1016/j.ecss.2021.107167

Russoniello, C. J., Konikow, L. F., Kroeger, K. D., Fernandez, C., Andres, A. S., & Michael, H. A. (2016). Hydrogeologic controls on groundwater discharge and nitrogen loads in a coastal watershed. *Journal of Hydrology*, *538*, 783–793. https://doi.org/10.1016/j.jhydrol.2016.05.013

Santoro, A. E. (2010). Microbial nitrogen cycling at the saltwater – Freshwater interface. *Hydrogeology Journal*, *18*(1), 187–202. https://doi.org/10.1007/s10040-009-0526-z

Santoro, A. E., Sakamoto, C. M., Smith, J. M., Plant, J. N., Gehman, A. L., Worden, A. Z., et al. (2013). Measurements of nitrite production in and around the primary nitrite maximum in the central California Current. *Biogeosciences*, *10*(11), 7395–7410. https://doi.org/10.5194/bg-10-7395-2013

Santos, I. R., Burnett, W. C., Chanton, J., Mwashote, B., Suryaputra, I. G. N. A., & Dittmar, T. (2008). Nutrient biogeochemistry in a Gulf of Mexico subterranean estuary and groundwater-derived fluxes to the coastal ocean. *Limnology & Oceanography*, *53*(2), 705–718. https://doi.org/10.4319/lo.2008.53.2.0705

Santos, I. R., Burnett, W. C., Dittmar, T., Suryaputra, I. G. N. A., & Chanton, J. (2009). Tidal pumping drives nutrient and dissolved organic matter dynamics in a Gulf of Mexico subterranean estuary. *Geochimica et Cosmochimica Acta*, *73*(5), 1325–1339. https://doi.org/10.1016/j.gca.2008.11.029

Santos, I. R., Chen, X., Lecher, A., Sawyer, A., Moosdorf, N., Rondellas, V., et al. (2021). Submarine groundwater discharge impacts on coastal nutrient biogeochemistry. *Nature Reviews Earth and Environment*, *2*(5), 307–323. https://doi.org/10.1016/B978-0-12-409548-9.11482-4

Schutte, C. A., Wilson, A. M., Evans, T., Moore, W. S., & Joye, S. B. (2017). Deep oxygen penetration drives nitrification in intertidal beach sands. *Limnology & Oceanography*, *63*(00), 1–16. https://doi.org/10.1002/lno.10731

Shrivastava, S., Stewardson, M. J., & Arora, M. (2021). Influence of bioturbation on hyporheic exchange in streams: Conceptual model and insights from laboratory experiments. *Water Resources Research*, *57*(2), 1–18. https://doi.org/10.1029/2020WR028468

Sigman, D. M., Casciotti, K. L., Andreani, M., Barford, C., Galanter, M., & Bohlke, J. K. (2001). A bacterial method for the nitrogen isotopic analysis of nitrate in seawater and freshwater. *Analytical Chemistry*, *73*(17), 4145–4153. https://doi.org/10.1021/ac010088e

Slomp, C. P., & Cappellen, P. V. (2004). Nutrient inputs to the coastal ocean through submarine groundwater discharge: Controls and potential impact. *Journal of Hydrology*, *295*(1–4), 64–86. https://doi.org/10.1016/j.jhydrol.2004.02.018

Smith, R. L., Baumgartner, L. K., Miller, D. N., Repert, D. A., & Böhlke, J. K. (2006). Assessment of nitrification potential in ground water using short term, single-well injection experiments. *Microbial Ecology*, *51*(1), 22–35. https://doi.org/10.1007/s00248-004-0159-7

Smith, R. L., Bohlke, J. K., Song, B., & Tobias, C. R. (2015). Role of anaerobic ammonium oxidation (Anammox) in nitrogen removal from a freshwater aquifer. *Environmental Science and Technology*, *49*(20), 12169–12177. https://doi.org/10.1021/acs.est.5b02488

21698961, 2024, 6, Downloaded from https://agupubs.onlinelibrary.wiley.com/doi/10.1029/2023JG007876 by Viva Jmu Procurement Services, Wiley Online Library on [30/03/2025]. See the Terms and Conditions (https://onlinelibrary.wiley.com/terms-and-conditions) on Wiley Online Library for rules of use; OA articles are governed by the applicable Creative Commons License

Tobias, C. R., Bohlke, J. K., Harvey, J. W., & Busenberg, E. (2009). A simple technique for continuous measurement of time-variable gas transfer in surface waters. *Limnology and Oceanography*, *7*(2), 185–195. https://doi.org/10.4319/lom.2009.7.185

Ullman, W. J., Chang, B., Miller, D. C., & Madsen, J. A. (2003). Groundwater mixing, nutrient diagenesis, and discharges across a sandy beachface Cape Henlopen, Delaware (USA). *Estuarine, Coastal and Shelf Science*, *57*(3), 539–552. https://doi.org/10.1016/S0272-7714(02)00398-0

Usui, T., Koike, I., & Ogura, N. (2001). N_2O production, nitrification and denitrification in an estuarine sediment. *Estuarine, Coastal and Shelf Science*, *52*(6), 769–781. https://doi.org/10.1006/ecss.2000.0765

Valiela, I., Collins, G., Kremer, J., Lajtha, K., Geist, M., Seely, B., et al. (1997). Nitrogen loading from coastal watersheds. *Ecological Applications*, *7*(2), 358–380. https://doi.org/10.2307/2269505

Valiela, I., Costa, J., Foreman, K., Teal, J. M., Howes, B., & Aubrey, D. (1990). Transport of groundwater-borne nutrients from watersheds and their effects on coastal waters. *Biogeochemistry*, *10*(3), 177–197. https://doi.org/10.1007/BF00003143

Wankel, S. D., Mosier, A. C., Hansel, C. M., Paytan, A., & Francis, C. A. (2011). Spatial variability in nitrification rates and ammonia-oxidizing microbial communities in the agriculturally impacted Elkhorn Slough estuary, California. *Applied and Environmental Microbiology*, *77*(1), 269–280. https://doi.org/10.1128/AEM.01318-10

Ward, B. B. (2011). Measurement and distribution of nitrification rates in the oceans. In *Methods in enzymology* (1st ed., Vol. 486, pp. 307–323). Elsevier Inc. https://doi.org/10.1016/B978-0-12-381294-0.00013-4

Ward, B. B. (2013). Nitrification. In *Encyclopedia of ecology* (pp. 351–358). https://doi.org/10.1016/B978-0-12-409548-9.00697-7

Wilson, S. J., Anderson, I. C., & Song, B. (2023). Geochemical factors impacting nitrifying communities Insandy sediments. *Environmental Microbiology*, *25*(12), 3180–3191. https://doi.org/10.1111/1462-2920.16504

Wilson, S. J., Anderson, I. C., Song, B., & Tobias, C. R. (2023). Temporal and spatial variation in subterranean estuary geochemical gradients and nutrient cycling rates: Impacts on groundwater nutrient export to estuaries. *Biogeosciences*, *128*(6), e2022JG007132. https://doi.org/10.1029/2022JG007132

Wilson, S. J., Moody, A., McKenzie, T., Cardenas, M. B., Luijendijk, E., Sawyer, A. H., et al. (2024). Global subterranean estuaries modify groundwater nutrient loading to the ocean. *Limnology and Oceanography Letters*. https://doi.org/10.1002/lol2.10390

21698961, 2024, 6, Downloaded from https://agupubs.onlinelibrary.wiley.com/doi/10.1029/2023JG007876 by Viva Jmu Procurement Services, Wiley Online Library on [30/03/2025]. See the Terms and Conditions (https://onlinelibrary.wiley.com/terms-and-conditions) on Wiley Online Library for rules of use; OA articles are governed by the applicable Creative Commons License